Available online at www.sciencedirect.com
SCIENCE DIRECT
Solid State Ionics 177 (2006) 907–913
SOLID STATE IONICS
www.elsevier.com/locate/ssi

Electrode reaction of $Sr_{1-x}La_xCo_{0.8}Fe_{0.2}O_{3-\delta}$ with $x=0.1$ and 0.6 on $Ce_{0.9}Gd_{0.1}O_{1.95}$ at $600 \leq T \leq 800$ °C

N. Grunbaum [a], L. Dessemond [b,*], J. Fouletier [b], F. Prado [a], A. Caneiro [a]

[a] Centro Atómico Bariloche, CNEA, 8400 S. C. de Bariloche RN, Argentina
[b] Laboratoire d'Electrochimie et de Physicochimie des Matériaux et des Interfaces (L.E.P.M.I), E.N.S.E.E.G., I. N. P. Grenoble, BP 75, 38402 Saint Martin d'Heres Cedex, France

Received 10 October 2005; received in revised form 13 January 2006; accepted 7 February 2006

Abstract

The electrode reaction of the perovskite phases $Sr_{1-x}La_xCo_{0.8}Fe_{0.2}O_{3-\delta}$ ($x=0.1$ and 0.6) on $Ce_{0.9}Gd_{0.1}O_{1.95}$ has been investigated by impedance spectroscopy in the temperature range $600 \leq T \leq 800$ °C. Thick porous electrodes ($t \sim 20$ μm) were sprayed on $Ce_{0.9}Gd_{0.1}O_{1.95}$ and ac impedance spectra were recorded on symmetrical cells at the equilibrium. The analysis of the complex impedance diagrams clearly indicates the presence of two contributions. The low frequency one was assigned to the gas phase oxygen diffusion through the porous electrode and a finite length diffusion (Warburg) impedance was used to describe the high frequency (HF) data. The polarization resistance of the HF impedance contribution (R_w) is higher for $x=0.1$ while the activation energy of R_w is higher for $x=0.6$. The variations of R_w versus the La content, temperature and thickness indicate that the Warburg-type impedance contains information of both bulk oxygen diffusion and surface processes.

Keywords: Mixed conductors; Electrode reaction; Cobaltites; SOFC; Impedance spectroscopy

1. Introduction

Solid oxide fuel cells (SOFC) are regarded as a feasible technology for generating electricity from hydrogen or hydrocarbon fuels. Nowadays, one of the main research efforts is devoted to decrease the SOFC operating temperature [1,2]. To reach this objective a new set of materials including electrolyte and electrodes should be considered to improve the performance in the temperature range $500 \leq T \leq 700$ °C with respect to the SOFC based on yttria stabilized zirconia (YSZ). Among the electrolytes, gadolinia-doped ceria $Ce_{1-x}Gd_xO_{2-x/2}$ (CGO) with $x \sim 0.1$ is a strong candidate to replace YSZ [1–3]. Concerning cathodes, the perovskite phases $(La,Sr)(Fe,Co)O_3$ (LSCF) fulfill the requirements of high electronic (σ_e) and ionic (σ_i) conductivities [4,5], good catalytic activity [6], high oxygen permeability [7] and are chemically and thermally compatible with CGO [8,9]. Accordingly, lanthanum ferrite-based perovskites are the most promising cathode materials for intermediate temperature SOFC (IT-SOFC) [10,11]. It is known that the ionic conductivity σ_i in the LSCF system increases with Sr and Co contents [4,5] whereas there is an opposite tendency for chemical stability [12,13]. Indeed, the limit compound $SrCoO_{3-\delta}$ is a mixture of two phases at room temperature: the $Sr_6Co_5O_{13}$ phase with a hexagonal crystal structure and the spinel phase Co_3O_4 [14]. The substitution of Fe for Co helps to stabilize the pseudo-cubic structure at lower temperatures for high Sr contents [15]. In particular, the $SrCo_{0.8}Fe_{0.2}O_{3-\delta}$ compound was found to exhibit a $\sigma_i \sim 1$ S cm^{-1} at 800 °C in air [4], related to the large oxygen nonstoichiometry (δ) that this phase is able to accommodate [15,16]. However, the large concentration of oxygen vacancies yields a structural transformation from a cubic or pseudo-cubic phase to the brownmillerite phase with orthorhombic symmetry, which can be hindered by the partial substitution of La for Sr [17]. As for ionic conductivity, the thermal expansion coefficient of the perovskite phases also increases with Sr and Co contents [18], yielding thermal mismatch between CGO and the cathode layer.

Since LSCF can be regarded as a mixed ionic electronic conductor above typically 600 °C [19], large oxygen fluxes are

* Corresponding author. Tel.: +33 4 76 82 65 65; fax: +33 4 76 82 66 70.
E-mail address: Laurent.Dessemond@lepmi.inpg.fr (L. Dessemond).

0167-2738/$ - see front matter © 2006 Elsevier B.V. All rights reserved.
doi:10.1016/j.ssi.2006.02.009

expected and electrode losses should be lowered compared with electrodes where the reaction occurs only at the three phase boundary (TPB) points. Recently, the behaviour of MIEC cathode materials has been numerically modeled [20]. The reported results suggest that the electrochemically active zone is broadened by increasing the ionic conductivity of the electrode material, although it is still confined in the vicinity of the TPB. Accordingly, enhancing ionic conductivity without deterioration of chemical stability should reduce electrode polarization losses.

The electrode characterization of LSCF cathodes on CGO electrolytes has been mainly performed on porous cathodes with high La and Fe contents, emphasizing that composite electrodes yield better performances [21,22]. However, few information is available on perovskite phases with high Sr and/or Co contents [23,24]. Thus, in this study, the polarization resistance of thick porous electrodes of $Sr_{1-x}La_xCo_{0.8}Fe_{0.2}O_{3-\delta}$ with $x=0.1$ and 0.6 sprayed on $Ce_{0.9}Gd_{0.1}O_{1.95}$ was determined by impedance spectroscopy between 600 and 800 °C.

2. Experimental

The $Sr_{1-x}La_xCo_{0.8}Fe_{0.2}O_{3-\delta}$ samples with $x=0.1$ and 0.6 were prepared by an acetic acid-based gel route [25]. Stoichiometric amounts of $SrCO_3$, La_2O_3, $Fe(CH_3COO)_2$, and $Co(CH_3COO)_2\cdot 4H_2O$ were weighed and dissolved in acetic acid. With the addition of water and small amounts of hydrogen peroxide, the mixture was refluxed at $T\sim 80$ °C until a clear solution was obtained. Then, solvents were evaporated in a hot plate to form a reddish transparent gel, which was first dried and subsequently decomposed at 400 °C during 30 min. The resulting powder was fired at 900 °C during 24 h in air. At this stage, the formation of perovskite phases was checked by X-ray powder diffraction.

The ink for electrode deposition was prepared mixing the as prepared powder with ethanol, terpineol, polyvinyl butyral, and polyvinyl pyrridone in appropriate ratio. The electrolyte $Ce_{0.9}Gd_{0.1}O_{1.95}$ (CGO) was prepared by the solid state reaction method. Stoichiometric quantities of highly pure CeO_2 and Gd_2O_3 were weighed and then ground by ball milling during 1 h. The powder was then pressed uniaxially into 12.5 mm diameter discs, ~1 mm thick and fired at 1600 °C during 6 h in air. After sintering, the diameter of the pellets was 11 mm.

The electrochemical cell was prepared with the symmetrical configuration. Both sides of the electrolyte were rectified before spraying the cathode ink on them. Afterwards these assemblies were heat treated at 1000 °C for 1 h in air to reach a sufficient adherence between electrodes and electrolyte. The heating rate was 4 °C/min, while the cooling rate was of 10 °C/min. The reported procedure was the same for both compounds.

The formation of the perovskite phase was verified by means of powder X-ray diffraction (XRD) measurements ($10\le 2\theta\le 70°$) by using a Philips PW1700 diffractometer with Cu–K_α radiation and a graphite monochromator. The thickness and morphology of the electrodes were determined with a Philips 515 scanning electron microscopy (SEM).

Impedance spectroscopy measurements were carried out on heating from 600 to 800 °C in air, by steps of 50 °C, by using a potentiostat/impedance analyzer Autolab (Eco Chemie BV) between 10^{-3} and 10^4 Hz. In addition, electrochemical measurements were also performed at 600 °C at pO_2 values ranging from 1.5 10^{-3} to 1 atm. The oxygen partial pressure was monitored by mixing O_2 and Ar (or He) by means of an electrochemical pump and an oxygen gauge [26]. The gas flow rate was fixed equal to 100 mL/min. An ac signal of amplitude equal to 50 mV was applied to the cell, under zero DC polarization, in respect of the linearity of the electrical response. Platinum grids, slightly pressed on porous electrodes, were used as current collectors. Impedance diagrams were resolved using EQUIVCRT software [27].

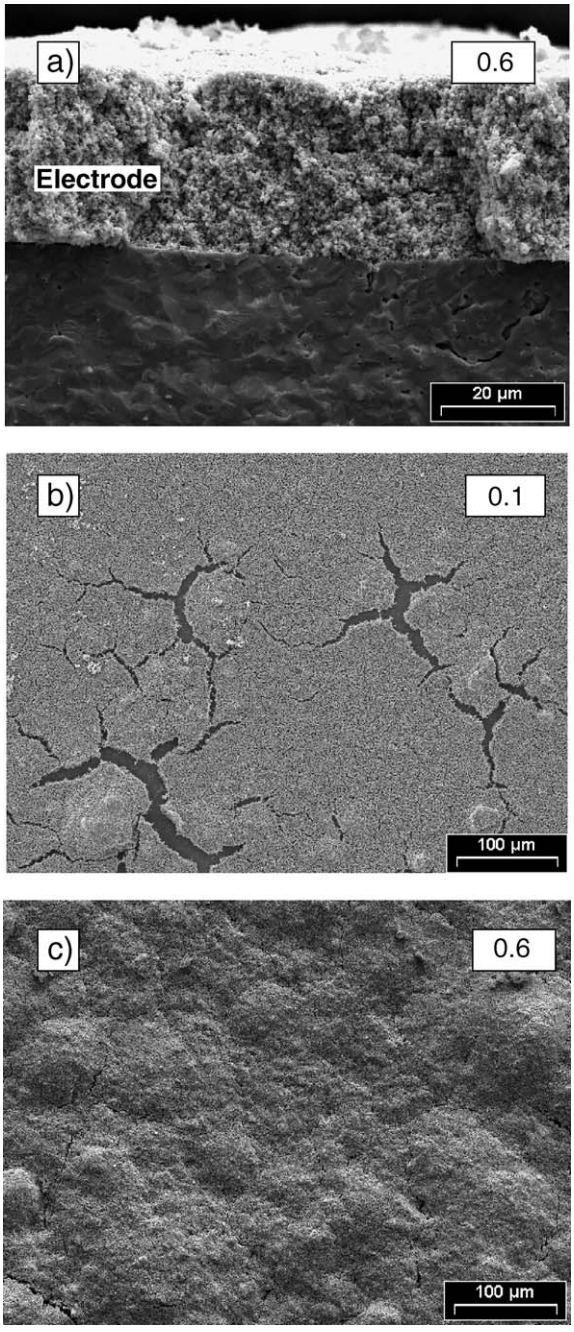

Fig. 1. Scanning electron micrographs: a) cross-section of the $x=0.6$ electrode, surface of the electrodes, b) $x=0.1$ and c) $x=0.6$.

3. Results and discussion

In Fig. 1a is presented a scanning electron micrograph of the cross-section of the $x=0.6$ electrode, which shows that the electrode adheres well on the electrolyte after the heat treatment at 1000 °C. The electrode thickness determined from SEM observations was in the range 15–20 μm for both samples.

The difference in the thermal expansion coefficients [18,24] with CGO [28] impeded the adherence of the $x=0$ cathode layer to the electrolyte. By other side, it was possible to attach the $x=0.1$ layer to the electrolyte allowing the impedance spectroscopy measurements. Another observation related with the microstructure of the electrodes was the presence of many cracks in the $x=0.1$ layer (Fig. 1b). The density and magnitude of the cracks clearly decrease for the $x=0.6$ layer (Fig. 1c). The origin of these cracks may be related with differences in the shrinkage during the heat treatment performed at 1000 °C. The formation of the perovskite phase was checked by X-ray powder diffraction. The main reflections were assigned to the perovskite phases and weak ones to the electrolyte below the porous films. No secondary phases were detected.

The evolution with temperature of impedance diagrams for $Sr_{0.9}La_{0.1}Co_{0.8}Fe_{0.2}O_{3-\delta}$ and $Sr_{0.4}La_{0.6}Co_{0.8}Fe_{0.2}O_{3-\delta}$, respectively is shown in Fig. 2. The shape of experimental impedance diagrams is rather similar to those previously reported in the literature [10,21,29]. The low temperature ($T=600$ °C) spectra clearly show the contribution of at least two processes referred as low frequency (LF) or high frequency (HF) depending on the frequency range within they are described. Accordingly, electrode impedance diagrams were fitted to an equivalent circuit containing two distributed elements. The high frequency intercept of the electrode impedance on the real axis can be unambiguously related to the total resistance of the CGO pellet. The oxygen reduction mechanism on porous MIEC electrodes may involve several processes such as charge transfer at the current collector/electrode interface and electrode/electrolyte interfaces, oxygen exchange at the electrode surface, bulk and surface diffusion of oxygen species and gas phase diffusion.

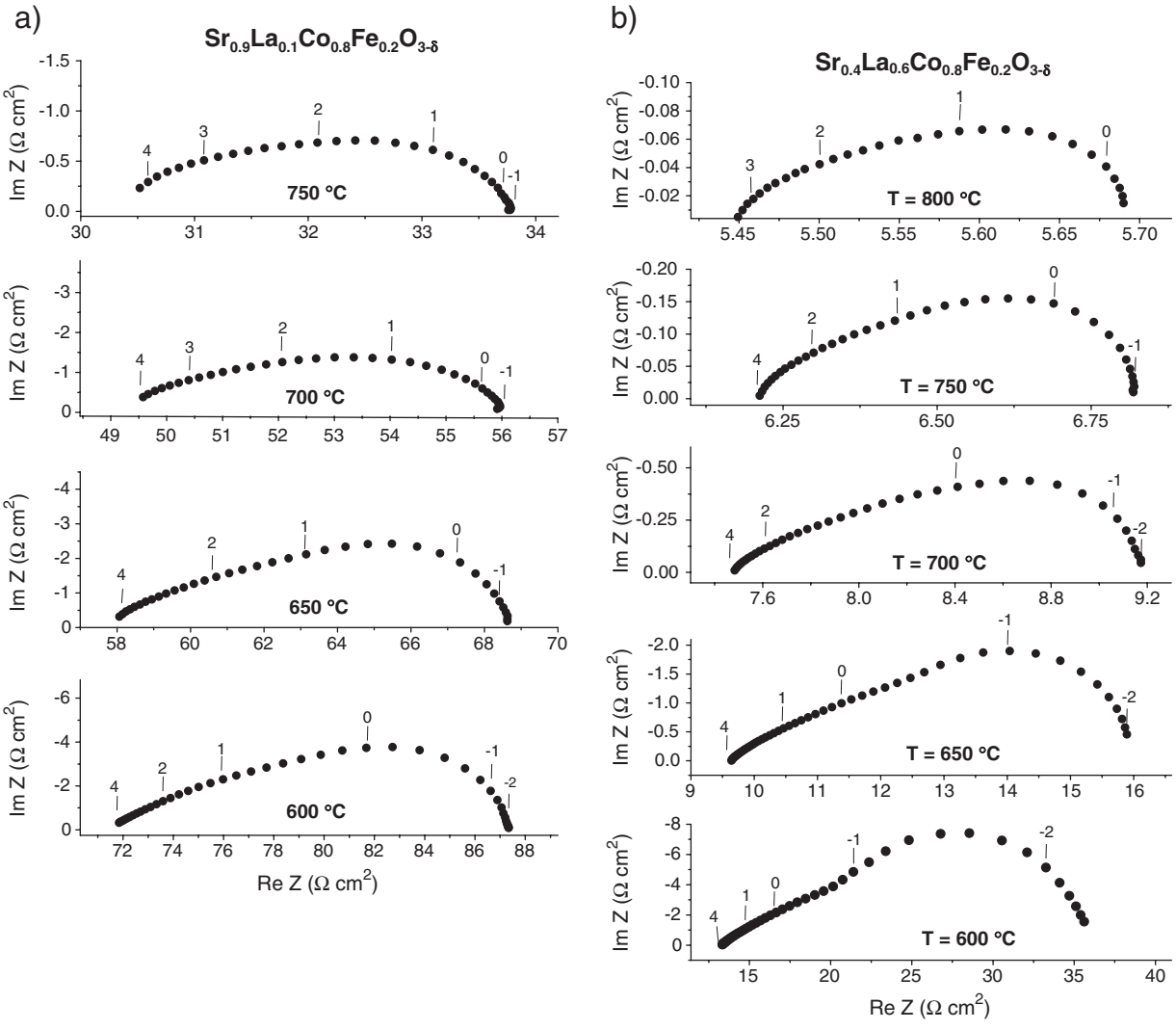

Fig. 2. Evolution of the impedance spectra with temperature, in air ($pO_2=0.209$ atm), for the $x=0.1$ and 0.6 electrodes. The numbers indicate the logarithm of the measuring frequency.

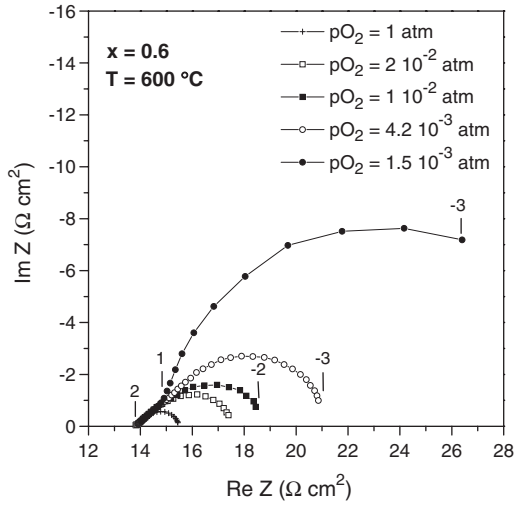

Fig. 3. Variation of the complex impedance spectra with the pO_2 at 600 °C for the $x=0.6$ electrode. The numbers indicate the logarithm of the measuring frequency.

Moreover, the effectiveness of the MIEC/gas interface can be influenced by these sequential processes [30].

Regardless of both lanthanum content of the electrode and oxygen partial pressure, the electrode impedance is always composed of a straight line at the highest frequencies (Figs. 2 and 3). At temperatures higher than 700 °C, the high frequency straight line fades away due to an increasing effect of the wires' inductance with a decreasing electrode resistance. In the absence of any significant additional high frequency semicircle on experimental impedance diagrams, one can assume that the electron transfer and ion transfer processes, occurring at the current collector/electrode and electrode/electrolyte interfaces, respectively, are sufficiently fast [31,32] and thus can be neglected. In case of cathodes with mixed conductivity, the whole electrode/electrolyte contact area can be used for the oxygen transfer if solid state diffusion through the electrode material can take place.

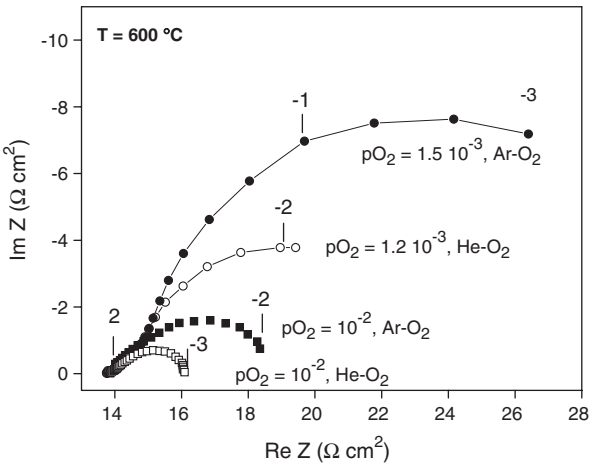

Fig. 4. Complex impedance diagrams of the $x=0.6$ electrode recorded at 600 °C under pO_2 values of 10^{-2} and $\sim 10^{-3}$ atm. The gas atmospheres were prepared by mixing O_2 and Ar or O_2 and He. The numbers indicate the logarithm of the measuring frequency.

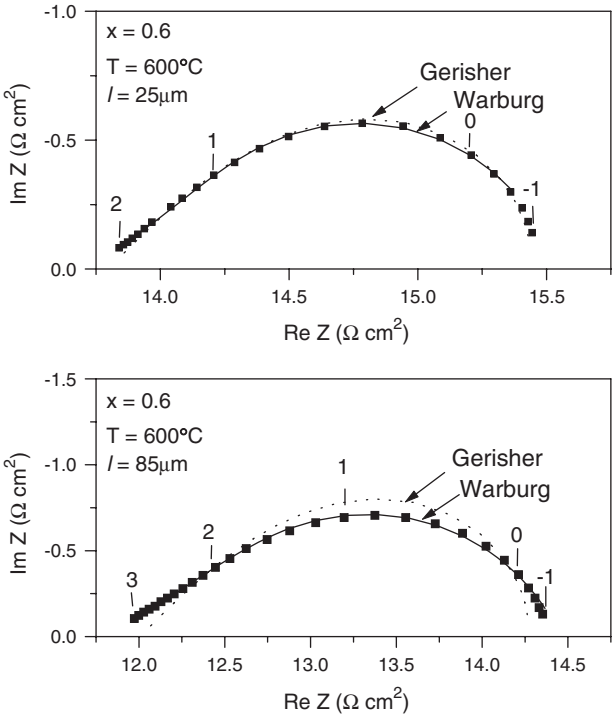

Fig. 5. Complex impedance diagrams recorded at 600 °C under pure O_2 ($pO_2=1$ atm) of the $x=0.6$ electrode with a thickness of 20 µm and 85 µm. The solid line corresponds to the fit of the experimental data with a Warburg-type impedance and the dashed line to the fit with a Gerisher-type impedance. The numbers indicate the logarithm of the measuring frequency.

As shown in Fig. 3, the magnitude of the LF contribution is a decreasing function of the oxygen partial pressure and it vanishes under pure O_2, while the high frequency part of the impedance remains unchanged. The low frequency extra arc was best fitted to an equivalent circuit consisting of a parallel combination of a resistance and a constant phase element $Z_{CPE}=1/(j\omega)^p$. The experimental p values are typically higher than 0.9, which is close to the value for a pure capacitance ($p=1$) as could be expected for gas phase diffusion polarization [33]. Moreover, the low frequency resistance depends on the gas component: replacement of Ar with He decreases the LF resistance because of a higher effective O_2 diffusivity in the He–O_2 mixture [34]. Fig. 4 shows this behaviour in the case of the $x=0.6$ sample at 600 °C for the pO_2 values 10^{-2} and $\sim 10^{-3}$ atm. All these results infer that the low frequency contribution in the electrode characteristic of LSCF compounds can be primarily attributed to gas phase diffusion. Nevertheless, since the gas flow rate was kept constant during experiments (as well as the apparatus geometry), one can not distinguish between boundary layer diffusion above the porous electrode (and through the current collector) [35] and pore diffusion through the porous electrode [34]. Impedance diagrams reveal that gas phase diffusion is evident even in air at 600 °C (Fig. 2).

Without any gas phase diffusion limitations (i.e. under pure oxygen), the impedance of MIEC based cathodes has the form of a Gerischer-type impedance one [31]. Nevertheless, the straight line can be also regarded as the high frequency characteristic of a finite-length diffusion process which can be

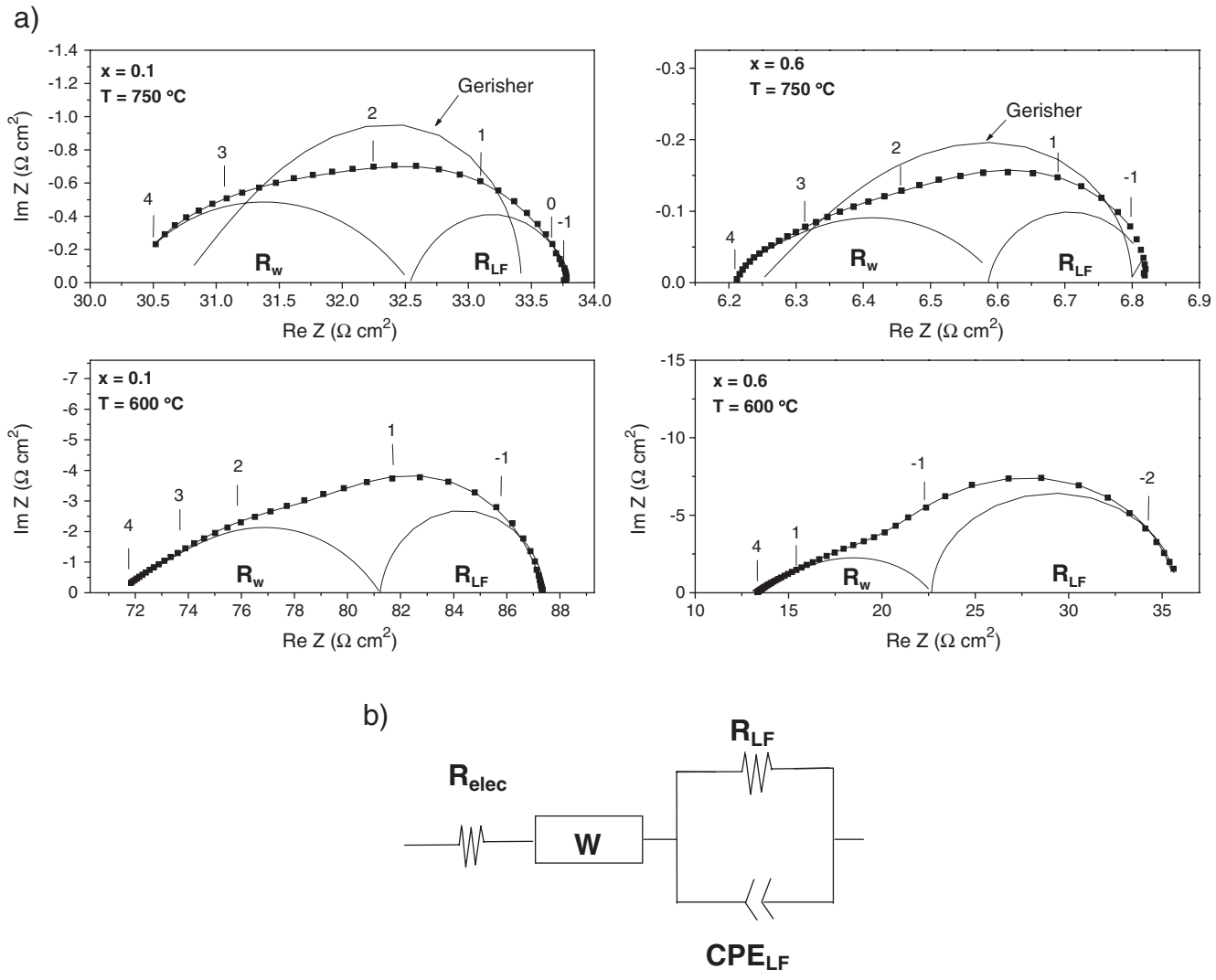

Fig. 6. a) Complex impedance diagrams recorded at 600 and 750 °C in air (pO_2=0.209) for both electrodes fitted with a Warburg-type impedance at HF and a circuit element of a resistance and a capacitor at LF. The numbers indicate the logarithm of the measuring frequency. b) Equivalent circuit of the electrode reaction.

related to a Warburg-type impedance [36]. In the latter case, the expression of the electrode impedance is [37]:

$$Z_W(\omega) = \frac{RT}{4F^2}\frac{1}{SC_0}\frac{th(l\sqrt{j\omega/D_v})}{\sqrt{j\omega D_v}} \quad (1)$$

where R and F are the gas and Faraday constants, S the electrode/electrolyte interface area, C_0 the oxygen vacancy concentration in equilibrium with air, D_v the oxygen vacancy diffusion coefficient, ω the angular frequency.

In case of dense electrodes, l is determined by the electrode thickness while for porous ones, it represents a characteristic length describing the size of the region where the electrode reaction is active [31]. The corresponding polarization resistance (Warburg resistance R_w) depends linearly on l according:

$$R_W = \frac{RT}{4F^2}\frac{1}{SC_0}\frac{l}{D_v} \quad (2)$$

Under pure oxygen, when the gas phase diffusion contribution to the electrode resistance is eliminated, impedance diagrams were analyzed according to a Gerischer- or a Warbug-type impedance (Fig. 5). The best fit was obtained with the latter approach. A similar description of the HF contribution of the LSCF impedances has been performed in air (Fig. 6a). Accordingly, experimental data were best fitted to an equivalent circuit consisting of a series association of a high frequency Warburg-type impedance and a low frequency semicircle related to the gas phase diffusion process. This result indicates that solid state diffusion through LSCF is one of the elementary processes of the electrode reaction mechanism. It is worth mentioning that the existence of only one Warburg-type impedance does not ensure that bulk diffusion is mainly the rate determining step of the electrode reaction. According to theoretical predictions [38], such an impedance contribution can be recorded at the equilibrium even if the O_2 reduction is limited by an interfacial step and solid state diffusion, in agreement with the results of Adler [31]. The occurrence of a mixed kinetics control of the oxygen reduction has been already emphasized from oxygen permeation measurements through (La,Sr)(Co,Fe)O_3 perovskite-type oxides [39,40]. According to experimental data on Fig. 5, one can deduce that the electrode resistance increases with the

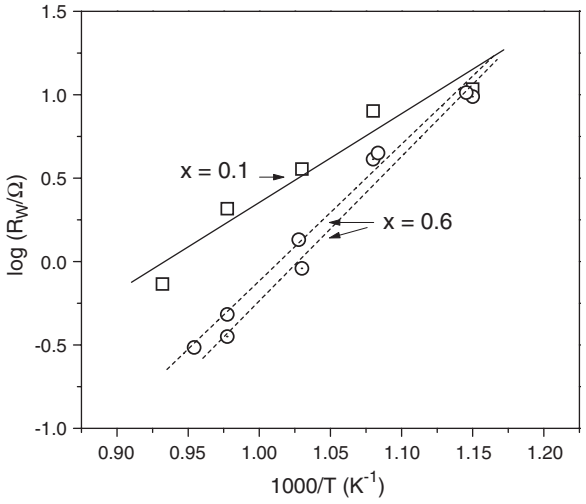

Fig. 7. Arrhenius plot of the Warburg resistance R_w obtained for the $Sr_{1-x}La_xCo_{0.8}Fe_{0.2}O_{3-\delta}$ electrode with $x=0.1$ and 0.6 in air ($pO_2=0.209$ atm).

electrode thickness in rather well agreement with Eq. (2), as already reported for strontium-doped manganite and cobaltite dense electrodes [36,41]. This result suggests that the electrode kinetics is not dominated by the TPB points [30]. Although only two points are available, a resistance can be deduced from extrapolation to zero thickness. This residual resistance could be attributed to the interfacial step at the gas/electrode interface, further suggesting a mixed kinetic control of the electrode reaction. Since the gas phase diffusion resistance depends on several microstructural parameters [42,43], which were not controlled in the investigated samples, we will focus now our discussion on the behaviour of the Warburg resistance.

Fig. 7 shows the Arrhenius plot of R_w for $Sr_{0.9}La_{0.1}Co_{0.8}Fe_{0.2}O_{3-\delta}$ and $Sr_{0.4}La_{0.6}Co_{0.8}Fe_{0.2}O_{3-\delta}$ electrodes. The reproducibility of the experimental data is shown in Fig. 7 by plotting R_w values obtained for two samples with the same La content ($x=0.6$). The related activation energy value is $E_a=1.0$ eV for $x=0.1$ and $E_a=1.6$ eV for $x=0.6$, in agreement with those previously reported for the perovskite phases (La,Sr)(Fe,Co)O_3 [36,44,45]. According to Eq. (2), R_w depends inversely on the oxygen vacancy concentration C_0 and the oxygen vacancy diffusion coefficient D_v. For a given temperature between 500 and 900 °C the oxygen non-stoichiometry for $Sr_{1-x}La_xCo_{0.8}Fe_{0.2}O_{3-\delta}$ electrodes ($0\le x\le 0.6$) increases monotonically as the La content decreases [17], which suggest that R_w should be lower for $x=0.1$. The fact that the R_w data show the opposite trend indicates that the variation of the Warburg resistance versus the lanthanum content may include other contributions of the oxygen reduction mechanism, further suggesting a mixed kinetic control. However, we do not rule out the influence of the electrode microstructure on R_w. Further work is needed to understand this behaviour.

4. Conclusion

Thick porous electrodes (thickness ~ 20 μm) of $Sr_{0.9}La_{0.1}Co_{0.8}Fe_{0.2}O_{3-\delta}$ and $Sr_{0.4}La_{0.6}Co_{0.8}Fe_{0.2}O_{3-\delta}$ were symmetrically sprayed on CGO pellets. Impedance spectroscopy data clearly indicate that the polarization resistance of $Sr_{1-x}La_xCo_{0.8}Fe_{0.2}O_{3-\delta}$ electrodes in air between 600 and 800 °C originates from two different contributions. At high frequencies, the complex impedance was simulated with a Warburg-type impedance that accounts for a finite length oxygen diffusion process. The low frequency contribution to the polarization resistance is due to a gas phase oxygen diffusion process. The variation of R_w with the La content, temperature and thickness indicates that surface processes are contained in the HF complex impedance besides lattice oxygen diffusion.

Acknowledgements

This work was supported by CNEA (Argentine Atomic Energy Commission), Fundación Antorchas (Grant No. 14056/16), ANPCyT through PICT 02-12-12455 and 03-12-14493 and Cooperation Program ECOS-SUD.

References

[1] S.J. Skinner, Int. J. Inorg. Mater. 3 (2001) 113.
[2] B.C.H. Steele, J. Mater. Sci. 36 (2001) 1053.
[3] J.M. Ralph, A.C. Schoeler, M. Krumpelt, J. Mater. Sci. 36 (2001) 1161.
[4] Y. Teraoka, T. Nobunaga, N. Yamazoe, Chem. Lett. (1988) 503.
[5] Y. Teraoka, H.M. Zhang, K. Okamoto, N. Yamazoe, Mater. Res. Bull. 23 (1988) 51.
[6] Y. Matsumoto, S. Yamada, T. Nishida, E. Sato, J. Electrochem. Soc. 127 (1999) 2360.
[7] Y. Teraoka, H.M. Zhang, S. Furukawa, N. Yamazoe, Chem. Lett. (1985) 1743.
[8] A. Tsoga, A. Gupta, A. Naoumidis, P. Nikolopoulos, Acta Mater. 48 (2000) 4709.
[9] G.C. Kostogloudis, C. Ftikos, Solid State Ionics 126 (1999) 143.
[10] A. Esquirol, N.P. Brandon, J.A. Kilner, M. Mogensen, J. Electrochem. Soc. 151 (2004) A1847.
[11] A. Mai, V.A.C. Haanapel, S. Uhlenbruck, F. Tietz, D. Stöver, Solid State Ionics 176 (2005) 1341.
[12] L.W. Tai, M.M. Nasrallah, H.U. Anderson, D.M. Sparlin, S.R. Sehlin, Solid State Ionics 76 (1995) 259.
[13] L.W. Tai, M.M. Nasrallah, H.U. Anderson, D.M. Sparlin, S.R. Sehlin, Solid State Ionics 76 (1995) 273.
[14] W.T.A. Harrison, S.L. Hegwood, A.J. Jacobson, J. Chem. Soc., Chem. Commun. (1995) 1953.
[15] N. Grunbaum, L. Mogni, F. Prado, A. Caneiro, J. Solid State Chem. 177 (2004) 2350.
[16] L.M. Liu, T.H. Lee, L. Qiu, Y.L. Yang, A.J. Jacobson, Mater. Res. Bull. 31 (1996) 29.
[17] F. Prado, N. Grunbaum, A. Caneiro, A. Manthiram, Solid State Ionics 167 (2004) 147.
[18] A. Petric, P. Huang, F. Tietz, Solid State Ionics 135 (2000) 719.
[19] D. Mantzavinos, A. Hartley, I.S. Mercalfe, M. Sahibzada, Solid State Ionics 134 (2000) 103.
[20] J. Fleig, J. Power Sources 105 (2002) 228.
[21] V. Dusastre, J.A. Kilner, Solid State Ionics 126 (1999) 163.
[22] E.P. Murray, M.J. Server, S.A. Barnett, Solid State Ionics 148 (2002) 27.
[23] P. Tsiakaras, G. Marnellos, C. Athanassou, M. Stoukides, J.E. ten Elshof, H.J.M. Bouwmeester, H. Verweij, Solid State Ionics 86–88 (1996) 1451.
[24] H.Y. Tu, Y. Takeda, N. Imanishi, O. Yamamoto, Solid State Ionics 117 (1999) 277.
[25] Y. Xia, T. Armstrong, F. Prado, A. Manthiram, Solid State Ionics 130 (2000) 81.
[26] A. Caneiro, M. Bonnat, J. Fouletier, J. Appl. Electrochem. 11 (1981) 83.
[27] B.A. Boukamp, Solid State Ionics 20 (1986) 31.

[28] V.V. Kharton, F.M. Figueiredo, L. Navarro, E.N. Naumovich, A.V. Kovalesky, A.A. Yaremchenko, A.P. Viskup, A. Carneiro, F.M.B. Marques, J.R. Frade, J. Mater. Sci. 36 (2001) 1105.
[29] S.P. Jiang, Solid State Ionics 146 (2002) 1.
[30] M. Liu, J. Electrochem. Soc. 145 (1998) 142.
[31] S.B. Adler, Solid State Ionics 111 (1998) 125.
[32] N. Imanishi, T. Matsumura, Y. Sumiya, K. Yoshimura, A. Hirano, Y. Takeda, D. Mori, R. Kanno, Solid State Ionics 174 (2004) 245.
[33] S.B. Adler, J.A. Lane, B.C.H. Steele, J. Electrochem Soc 143 (1996) 3554.
[34] K. Huang, J. Electrochem. Soc. 151 (2004) H117.
[35] S. Primdhal, M. Mogensen, J. Electrochem. Soc. 146 (1999) 2827.
[36] A. Ringuedé, J. Fouletier, Solid State Ionics 139 (2001) 167.
[37] I.D. Raistrick, J.R. Macdonald, D.R. Franceschetti, in: J.R. Macdonald (Ed.), Impedance Spectroscopy. Emphasizing Solid Materials and Systems, Chapter 2, John Wiley and Sons, New York, 1987.
[38] J. Deseure, Y. Bultel, L. Dessemond, E. Siebert, Solid State Ionics 176 (2005) 234.
[39] H.J.M. Bouwmeester, H. Kruidhof, A.J. Burggraaf, Solid State Ionics 72 (1994) 185.
[40] J.A. Lane, S.J. Benson, D. Waller, J.A. Kilner, Solid State Ionics 121 (1999) 201.
[41] T. Ioroi, T. Hara, Y. Uchimoto, Z. Ogumi, Z.I. Takehara, J. Electrochem. Soc 144 (1997) 1362.
[42] X. Xu, C. Xia, G. Xiao, D. Peng, Solid State Ionics 176 (2005) 1513.
[43] S.P. Yoon, S.W. Nam, J. Han, T.H. Lim, S.A. Hong, S.H. Hyun, Solid State Ionics 166 (2004) 1.
[44] M.T. Colomer, B.C.H. Steele, J.A. Kilner, Solid State Ionics 147 (2002) 41.
[45] A. Esquirol, J. Kilner, N. Brandon, Solid State Ionics 175 (2004) 63.